European Journal of Pharmaceutics and Biopharmaceutics 144 (2019) 40–49

Contents lists available at ScienceDirect

European Journal of Pharmaceutics and Biopharmaceutics

journal homepage: www.elsevier.com/locate/ejpb

Research paper

Zeta potential changing self-emulsifying drug delivery systems: A promising strategy to sequentially overcome mucus and epithelial barrier

Imran Nazir[a,b], Andrea Fürst[a], Noemi Lupo[a], Andrea Hupfauf[c], Ronald Gust[c], Andreas Bernkop-Schnürch[a,*]

[a] Center for Chemistry and Biomedicine, Department of Pharmaceutical Technology, Institute of Pharmacy, University of Innsbruck, Innrain 80-82, A-6020 Innsbruck, Austria
[b] Department of Pharmacy, COMSATS University Islamabad, Abbottabad Campus, 22060 Abbottabad, Pakistan
[c] Center for Chemistry and Biomedicine, Department of Pharmaceutical Chemistry, Institute of Pharmacy, University of Innsbruck, Innrain 80-82, A-6020 Innsbruck, Austria

ARTICLE INFO

Keywords:
Zeta potential change
Self-emulsifying drug delivery systems (SEDDS)
Flip-flop mechanism
Mucus permeation
Cellular uptake

ABSTRACT

Aim: The aim of the present study was to develop zeta potential changing self-emulsifying drug delivery systems (SEDDS) via a flip-flop mechanism in order to improve their mucus permeating and cellular uptake properties.
Methods: Phosphorylated serine-oleylamine (p-Ser-OA) conjugates were synthesized and incorporated into SEDDS at a concentration of 1% (v/v). Cytotoxic potential of p-Ser-OA and p-Ser-OA loaded SEDDS was investigated on Caco-2 cells. Phosphate release was evaluated using isolated as well as cell-associated intestinal alkaline phosphatase (AP). In parallel, change in zeta potential and amino group concentration on the surface of SEDDS was determined. Furthermore, mucus permeation and cellular uptake studies were performed.
Results: p-Ser-OA was synthesized by covalent attachment of serine (Ser) to oleylamine (OA) via a carbodiimide-mediated reaction followed by phosphorylation using phosphorous pentoxide (P_2O_5) and phosphoric acid (H_3PO_4). The chemical structure of p-Ser-OA was confirmed via FT-IR, ^{1}H NMR, ^{13}C NMR, ^{31}P NMR and mass spectroscopic analysis. p-Ser-OA loaded SEDDS exhibited a droplet size and zeta potential of 46.42 ± 0.35 nm and −11.53 mV, respectively. A significant amount of phosphate was released after incubation with isolated as well as cell-associated AP within 6 h and zeta potential raised up to −2.04 mV. p-Ser-OA loaded SEDDS showed improved mucus permeation in comparison to p-Ser-OA loaded SEDDS treated with AP. Moreover, cellular uptake increased almost 2-fold after phosphate cleavage using AP.
Conclusion: Findings of this study show that SEDDS changing their zeta potential via a flip-flop mechanism exhibit both high mucus permeating and high cellular uptake properties.

1. Introduction

A wide range of active pharmaceutical ingredients (APIs) is administered via the mucosal route offering the possibility for both a local drug targeting and systemic drug delivery [1–3]. Mucosal delivery of APIs, however, is prominently influenced by the mucus gel layer covering these epithelium. It is a robust barrier that can immobilize and remove pathogens and xenobiotics particularly when they exhibited cationic and hydrophobic surface properties. Apart from the mucus gel layer, the epithelium per se is another challenging barrier that needs to be overcome [4]. Strategies to overcome these barriers include the use of auxiliary agents such as mucolytic agents [5,6] and permeation enhancers [7] as well as the design of nanocarrier systems providing high mucus permeating and drug absorption improving properties. Most of these nanocarrier systems, however, are either highly mucus permeating or drug absorption enhancing as opposite properties are needed to overcome each of these barriers [8].

Hydrophilic and negatively charged nanocarriers permeate rapidly through the mucus barrier, whereas hydrophobic and less negatively or preferably positively charged nanocarriers interact much more efficiently with the absorption membrane [9,10]. To address this dilemma, the concept of zeta potential changing nanocarriers was pioneered by our research group [11]. According to this concept, nanocarriers exhibiting a negative zeta potential due to phosphate substructures on the surface were developed providing enhanced mucus permeation. AP expressed by epithelial cells can cleave off these phosphate

* Corresponding author.
E-mail address: andreas.bernkop@uibk.ac.at (A. Bernkop-Schnürch).

https://doi.org/10.1016/j.ejpb.2019.09.007
Received 27 July 2019; Received in revised form 3 September 2019; Accepted 6 September 2019
Available online 07 September 2019
0939-6411/

substructures when nanocarriers reach the epithelium and the change in zeta potential facilitates their cellular uptake. Following this strategy various zeta potential changing nanocarrier systems including polymeric nanoparticles, micelles and SEDDS have been developed [10,12]. From the industrial point of view SEDDS seem to be most promising as their scale-up and production is comparatively easy. Suchaoin et al. developed the very first zeta potential changing SEDDS displaying a minor change in zeta potential from just −1 to +1 mV [13]. Similarly, Salimi et al. developed very first zeta potential changing SEDDS using flip-flop mechanism where phosphate and amino substructures were both positioned within the polar head group of the surfactant showing a change in zeta potential from even −12 to +5 mV [14]. So far, however, no evidence has been provided that zeta potential changing SEDDS exhibit high mucus permeating properties before phosphate cleavage and improved cellular uptake properties after phosphate cleavage.

It was therefore the aim of the present study to develop zeta potential changing SEDDS via a flip-flop mechanism in order to evaluate their mucus permeating as well as cellular uptake properties before and after phosphate cleavage. Hence, p-Ser-OA conjugate was synthesized and incorporated into SEDDS. The phosphate cleavage on the surface of SEDDS was evaluated in the presence of isolated AP as well as on Caco-2 cells resulting in amino substructures flipping out on the surface. Moreover, mucus permeation and cellular uptake studies were subject to this investigation.

2. Materials and methods

2.1. Materials

Boc-serine (Ser), oleylamine (OA), phosphorus pentoxide (P_2O_5), 1-hydroxybenzotriazole (HOBt), ethyl acetate, deuterium chloride (DCl), sodium sulfate, Cremophore EL (polyethoxylated-35 castor oil, HLB = 13), 4-(2-hydroxyethyl)-1-piper-azineethanesulfonic acid (HEPES), alkaline phosphatase from bovine intestinal mucosa (isolated AP; 7165 unit/mg protein), phosphatase inhibitor cocktail 2, Triton X-100, sulfuric acid (H_2SO_4), malachite green oxalate salt, ammonium molybdate tetrahydrate, potassium phosphate mono-basic (KH_2PO_4), L-cysteine hydrochloride, 2,4,6–trinitrobenzene sulfonic acid (TNBS), propylene glycol and glycerol were purchased from Sigma-Aldrich (Vienna, Austria). 1-(3-Dimethylaminopropyl)-3-ethylcarbodiimide (EDC) was purchased from TCI Chemicals (Eschborn, Germany). Phosphoric acid (H_3PO_4) 85% aqueous solution was purchased from Alfa Aesar (Kandel, Germany). Labrasol (caprylocaproyl macrogol-8 glycerides, HLB = 12) was kindly donated by Gattefossé (Lyon, France). Captex 355 (caprylic/capric triglyceride), Capmul PG-2L (propylene glycol dilaurate) and Capmul MCM (caprylic/capric mono- and diglycerides, HLB = 6.7) were kindly provided by Abitech (Oberhausen, Germany). N, N-Dimethylformamide (DMF) and petroleum ether were obtained from Carl Roth (Graz, Austria). All other chemicals and reagents used were obtained from commercial sources being of analytical grade.

2.2. Methods

2.2.1. Synthesis and characterization of phosphorylated serine-oleylamine (p-Ser-OA) conjugate

2.2.1.1. Synthesis of tert-butyl-(3-hydroxy-1-(octadec-9-en-1-ylamino)-1-oxopropan-2-yl)carbamate (Boc-Ser-OA). Boc-Ser was covalently attached to OA via amide bond formation. In brief, 500 mg (2.4 mmol) of Boc-Ser was dissolved in 2 mL of DMF and cooled to 0 °C. Then, 490 mg (3.6 mmol) of HOBt and 563 mg (3.6 mmol) of EDC were added and stirred for 20 min at 0 °C. Afterwards, 648 mg (2.4 mmol) of OA was added dropwise under constant stirring for 20 min at 0 °C. The reaction mixture was kept under stirring at room temperature for 24 h. Then, 30 mL of demineralized water was added to the reaction mixture followed by adjusting the pH to 8 using 2 M NaOH and extracted with ethyl acetate. Subsequently, the organic phase was washed three times with 0.001 M HCl followed by three times washing with demineralized water. The organic phase was dried over sodium sulfate and the solvent was removed under reduced pressure (G3 Vertical Condenser Heidolph™; Heidolph, Schwabach, Germany). Boc-Ser-OA was further purified by column chromatography using 60–120 mesh silica gel and a mixture of petroleum ether and ethyl acetate 1:1 as mobile phase.

Yield: 350 mg (0.8 mmol), 33% as colorless semisolid.

FT-IR: $\bar{\nu}$ = 3322 m, br (NH); 2922 s (aliphatic CH); 2853 m (aliphatic CH); 1697 m (C = O); 1649 s (C = O); 1529 m; 1456 m; 1365 m; 1246 m; 1167 s; 1057 m.

^{1}H NMR (400 MHz, $CDCl_3$): δ = 0.85 – 0.91 (m, 3H, C*H*$_3$); 1.22 – 1.36 (m, 22H, C*H*$_2$); 1.46 (s, 9H, C*H*$_3$Boc); 1.46 – 1.52 (m, 2H, C*H*$_2$CH$_3$); 1.67 (br, s, 1H, OH); 1.92 – 2.06 (m, 4H, C*H*$_2$ besides C = C); 3.14 – 3.32 (m, 2H, C*H*$_2$NH); 3.59 – 3.68 (m, 1H, C*H*CH$_2$); 4.06 – 4.15 (m, 2H, C*H*$_2$CH); 5.30 – 5.40 (m, 2H, C*H* = C*H*); 5.57 (bs, 1H, N*H* BOC); 6.67 (bs, 1H, N*H*).

^{13}C NMR (100 MHz, $CDCl_3$): δ = 14.1 (1C, CH$_2$*C*H$_3$); 22.7 (1C, *C*H$_2$); 26.8 (1C, *C*H$_2$); 27.2 (1C, *C*H$_2$); 27.2 (1C, *C*H$_2$); 28.3 (3C, C*C*H$_3$ BOC); 29.2 (1C, *C*H$_2$); 29.3 (1C, *C*H$_2$); 29.4 (1C, *C*H$_2$); 29.4 (1C, *C*H$_2$); 29.5 (1C, *C*H$_2$); 29.7 (1C, *C*H$_2$); 29.7 (1C, *C*H$_2$); 29.8 (1C, *C*H$_2$); 29.8 (1C, *C*H$_2$); 31.9 (1C, *C*H$_2$); 39.5 (1C, *C*H$_2$NH); 54.5 (1C, *C*HNH); 62.9 (1C, *C*H$_2$OH); 80.6 (1C, CH$_3$*C* BOC); 129.8 (1C, H*C* = CH); 130.0 (1C, HC = *C*H); 156.4 (1C, N*C* = O Boc); 171.5 (1C, N*C* = O).

2.2.1.2. Synthesis of 2-ammonium-3-(octadec-9-en-1-ylamino)-3-oxopropyl hydrogen phosphate salt (p-Ser-OA). Phosphorylation of Boc-Ser-OA was carried out by dissolving 470 mg (1.1 mmol) in 2 mL of DMF under constant stirring and cooling the reaction mixture to 0 °C. Afterward, 426 mg (3.0 mmol) of P_2O_5 was dissolved in 1.5 mL of H_3PO_4 and added dropwise under continuous stirring at 0 °C. The reaction mixture was heated to 80 °C and stirred for 20 h. Then 30 mL of demineralized water was added to the mixture at 40 °C that was further stirred at 80 °C for 1 h. Subsequently, the reaction mixture was extracted three times with 30 mL of ethyl acetate. p-Ser-OA was obtained after washing the organic phase several times with demineralized water, drying over sodium sulfate and solvent evaporation *in vacuo*. The synthesis of p-Ser-OA is illustrated in Fig. 1.

Yield: 180 mg (0.3 mmol), 27% as colorless semisolid.

FT-IR: $\bar{\nu}$ = 3323 m (NH); 2920 s (aliphatic CH); 2851 s (aliphatic CH); 1666 s (C = O amide); 1563 m (amide 2); 1212 m; 1172 m; 1065 s; 1009 s; 970 m; 945 s.

^{1}H NMR (400 MHz, CD_3OD + 10% of DCl solution): δ = 0.91 (m, 3H, C*H*$_3$); 1.25 – 1.40 (m, 22H, C*H*$_2$); 1.50 – 1.60 (m, 2H, C*H*$_2$CH$_3$); 1.95 – 2.08 (m, 4H, C*H*$_2$ besides C = C); 3.24 (t, ^{3}J = 7.2 Hz, 2H, CH$_2$C*H*$_2$NH); 3.83 (dd, ^{3}J = 6.4 Hz, ^{3}J = 11.6 Hz, 1H, C*H*CH$_2$); 3.95 (dd, ^{3}J = 11.6 Hz, ^{3}J = 4.2 Hz, 1H, C*H*$_2$CH); 3.99 (dd, ^{3}J = 6.4 Hz, ^{3}J = 4.4 Hz, 1H, C*H*$_2$CH); 5.30–5.40 (m, 2H, C*H* = C*H*).

^{13}C NMR (100 MHz, CD_3OD + 10% of DCl solution): δ = 13.1 (1C, *C*H$_3$); 22.3 (1C, *C*H$_2$); 26.6 (1C, *C*H$_2$); 26.7 (1C, *C*H$_2$); 26.7 (1C, *C*H$_2$); 28.8 (1C, *C*H$_2$); 28.9 (1C, *C*H$_2$); 28.9 (1C, *C*H$_2$); 29.0 (1C, *C*H$_2$); 29.1 (1C, *C*H$_2$); 29.2 (1C, *C*H$_2$); 29.3 (1C, *C*H$_2$); 29.4 (1C, *C*H$_2$); 29.4 (1C, *C*H$_2$); 31.6 (1C, *C*H$_2$); 39.4 (1C, *C*H$_2$NH); 54.9 (1C, *C*HNH$_2$); 60.5 (1C, *C*H$_2$O); 129.5 (2C, H*C* = CH); 166.8 (1C, N*C* = O).

^{31}P NMR (162 MHz, CD_3OD + 10% of DCl solution): δ = 1.07 (phosphoric acid ester); – 12.45 (ammonium phosphate).

MS: 355.3488 (predicted: 435.29 $[M + H]^+$, $[M^+ - 80]$ (phosphate split off): 355.33).

2.2.1.3. Characterization. Boc-Ser-OA and p-Ser-OA were characterized by FT-IR, ^{1}H NMR and ^{13}C NMR spectroscopy. p-Ser-OA was further characterized by ^{31}P NMR and mass spectroscopy. FT-IR spectra were recorded on a Bruker ALPHA FT-IR apparatus equipped with a Platinum ATR module and with OPUS Spectroscopy Software, version 7. FT-IR

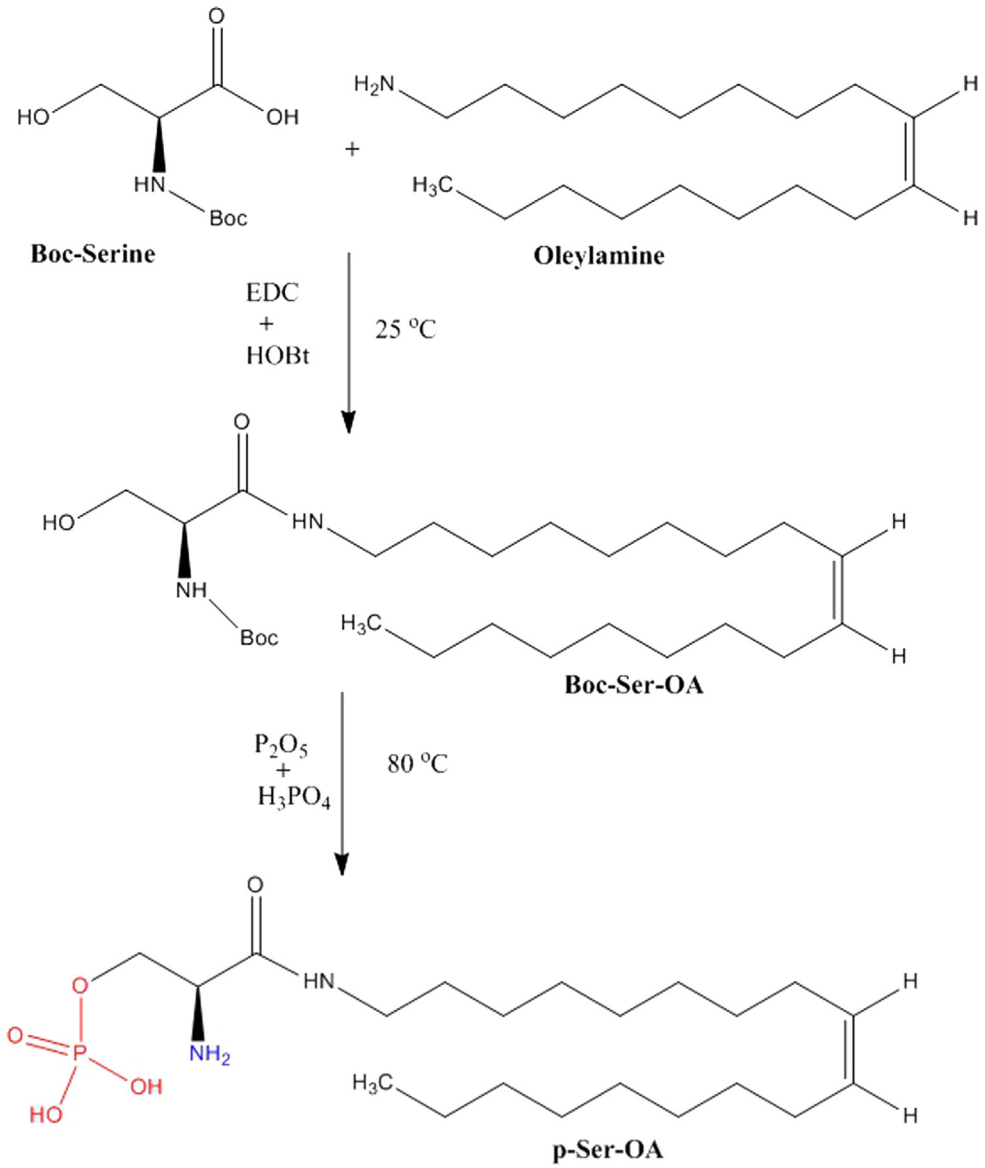

Fig. 1. Synthetic pathway for preparation of p-Ser-OA.

spectra of the samples were recorded with 24 scans at a resolution of 4 cm^{-1} in the wavenumber range from 4000 to 400 cm^{-1}. NMR spectra were recorded on a Bruker Avance 4 Neo spectrometer (^{1}H: 400.13 MHz, ^{13}C: 100.62 MHz, ^{31}P: 161.99 MHz). The center of the solvent signal and TMS signal were used as internal standard. Deuterated solvents were used to dissolve test samples. Mass spectra were recorded on a Thermo Fisher Orbitrap Elite, equipped with an ESI ion source.

2.2.2. SEDDS preparation and characterization

For the development of SEDDS formulations, various concentrations of oils, surfactants and co-surfactants were homogenized as listed in Table 1 using vortex mixer (Thermomixer comfort, Eppendorf, Germany) under constant shaking at 1000 rpm at 40 °C, whereby semisolid excipients were melted before use as described previously [15]. p-Ser-OA was incorporated up to 1% (v/v) in SEDDS pre-concentrates via ultra-sonication for 10 min at room temperature. The incorporation of p-Ser-OA into SEDDS pre-concentrate was evaluated visually after centrifugation at 12,100 g for 5 min. Aliquots of 100 µL of SEDDS pre-concentrates were emulsified in 10 mL of 100 mM HEPES buffer pH 7.0 containing 5 mM $MgCl_2$ and 0.2 mM $ZnCl_2$ before characterization.

Table 1
Composition of SEDDS formulations. Values are indicated in percent (v/v).

Formulations	FI	FII	FIII
Captex 355	30	–	–
Captex 300	–	–	25
Capmul MCM	20	30	–
Capmul PG 2L	–	–	25
Cremophore EL	30	30	30
Miglyol	–	20	–
Propylene glycol	10	20	20
Glycerol	10	–	–

Mean droplet size, polydispersity index (PDI) and zeta potential of blank as well as p-Ser-OA loaded SEDDS formulations were determined by photon correlation spectroscopy with Zetasizer Nano-ZSP (Malvern Instruments, Worcestershire, UK).

2.2.3. Cytotoxicity study

Cytotoxic potential of p-Ser-OA and p-Ser-OA loaded SEDDS was evaluated on Caco-2 cells using resazurin assay according to a previously described method [16]. Caco-2 cells were seeded in a 24-well

plate at a density of 2.5×10^4 cells/well in minimum essential medium (MEM) enriched with 10% (v/v) fetal bovine serum (FBS) and 1% penicillin/streptomycin solution (100 units/0.1 mg/L) being cultured at 37 °C in an atmosphere of 5% CO_2 and 95% relative humidity. MEM was changed every second day until a confluent monolayer of cells was obtained. Test solutions of p-Ser-OA were prepared in concentrations of 0.1% and 0.01% in 25 mM HEPES buffered saline (HBS) pH 7 containing 5% (v/v) ethanol and test solutions of SEDDS were prepared in dilutions of 1:50, 1:100, 1:300, 1:500 and 1:1000 in HBS. HBS buffer and 2% (v/v) Triton X-100 solution served as positive control and negative control, respectively. Cells were washed twice with preheated HBS at 37 °C before incubation with samples. Test solutions, positive control and negative control were added in triplicate to the cell culture plate in a volume of 500 µL/well and incubated at 37 °C. At predetermined time points (3 and 24 h), samples were removed and cells were washed twice with HBS. Aliquots of 500 µL of 2.2 mM resazurin solution were added to each well and incubated for 3 h. Thereafter, 100 µL were transferred to a 96-well black titer microplate and fluorescence intensity was measured at 540 nm excitation wavelength (λ_{ex}) and 590 nm emission wavelength (λ_{em}) using a microplate reader (Tecan Spark®, Tecan Trading AG, Zurich, Switzerland) in order to determine the degree of resazurin metabolism in Caco-2 cells. Cell viability was calculated using Eq. (1):

$$Cell\ \ viability = \left(\frac{sample\ \ flourescence - negative\ \ control\ \ flourescence}{positive\ \ control\ \ flourescence - negative\ \ control\ \ flourescence} \right) \times 100 \quad (1)$$

2.2.4. Enzymatic phosphate cleavage using isolated AP

Time-dependent phosphate cleavage of p-Ser-OA loaded SEDDS was investigated using isolated AP as described previously [14]. Briefly, 100 µL of isolated AP (10 U/mL) was added to 10 mL of p-Ser-OA loaded SEDDS diluted 1:1000 with 100 mM HEPES buffer pH 7 containing 5 mM $MgCl_2$ and 0.2 mM $ZnCl_2$. The solution was incubated at 37 °C under constant shaking at 400 rpm for 6 h. As a negative control, phosphate release from p-Ser-OA loaded SEDDS formulations was measured without adding isolated AP. At predetermined time points (0, 1, 2, 3, 4, 5 and 6 h), 50 µL of aliquots were withdrawn and enzymatic activity was stopped by addition of 5 µL of 3.6 M H_2SO_4. The amount of free inorganic phosphate was quantified by malachite green (MLG) assay.

In brief, 0.15% (m/v) MLG salt was dissolved in 3.6 M H_2SO_4. To 10 mL of MLG solution, 400 µL of 11% Triton X-100 solution was added and incubated at room temperature for 5 min in order to stabilize the MLG solution. Thereafter, 6 mL of 8% (m/v) ammonium molybdate solution was added dropwise under constant shaking. Samples were evaluated by addition of 100 µL of MLG reagent to 50 µL of withdrawn test samples. The amount of free phosphate was measured using a standard curve with an increasing amount of KH_2PO_4. MLG and phospho-molybdate complex was quantified by measuring absorbance at 630 nm with a microplate reader (Tecan Spark®, Tecan Trading AG, Zurich, Switzerland).

2.2.5. Enzymatic phosphate cleavage by Caco-2 cell monolayer

Time-dependent cleavage of the phosphate substructures of p-Ser-OA loaded SEDDS was performed on Caco-2 cell monolayer [13]. Cells were seeded in 24-well plates at a density of 2.5×10^4 cells/well as described above. MEM was changed every second day until a confluent monolayer of cells was obtained. Prior to experiments, cells were washed twice with HBS. Cells were pre-incubated with the phosphatase inhibitor cocktail or HBS for 1 h. Subsequently, Caco-2 cells were incubated with 500 µL of p-Ser-OA loaded SEDDS diluted 1:1000 in HBS. Aliquots of 50 µL were withdrawn from each well at predetermined time points and the enzymatic reaction was stopped by adding 5 µL of 3.6 M H_2SO_4. The amount of phosphate released was quantified by MLG assay. As a negative control, p-Ser-OA loaded SEDDS were diluted in the same ratio using buffer containing 1% phosphate inhibitor.

2.2.6. Mucus permeation behavior of SEDDS

In vitro mucus permeation behavior of SEDDS was evaluated in a similar way as developed by Friedl et al. via Transwell insert method [17]. The intestine of a freshly slaughtered pig was collected from a local slaughterhouse and stored on ice during transport to the laboratory. Intestinal segments containing chime were removed. The small intestine was incised longitudinally and debris was discarded by rinsing with ice-cold physiological saline solution. The mucus was gently scraped from the intestine and collected in a beaker. Thereafter, 5 mL of 0.1 M sodium chloride solution was added to 1 g of mucus and stirred for 1 h at 4 °C. The mixture was centrifuged at 10,400 g for 2 h at 10 °C. The supernatant was discarded and purified mucus was obtained. The purified mucus was stored at −20 °C prior to use.

For mucus permeation studies, 24-well Transwell plates with inserts having a surface of 33.6 mm^2 and pore size of 3 µm (Greiner Bio-One, Austria) were used and these inserts were covered with 70 mg of intestinal mucus. The acceptor chamber was filled with 500 µL of HBS. SEDDS was labeled by addition of FDA solution (1 mg/mL in DMSO) to SEDDS pre-concentrates in a final concentration of 0.5%. The donor chamber was filled with 250 µL of these FDA labeled SEDDS diluted 1:1000 in the same buffer. To eliminate the effect of the filter, SEDDS formulations were tested in parallel without mucus to obtain 100% reference value. Another control experiment was performed using buffer without the addition of any formulation serving as 0% reference value. As control, p-Ser-OA loaded SEDDS was pretreated with isolated AP. For pretreated SEDDS, 100 µL of the aqueous solution of AP (10 U/mL) was added to 10 mL of p-Ser-OA loaded SEDDS diluted 1:1000 in the same buffer and incubated at 37 °C under constant shaking at 400 rpm for 6 h. The plate was wrapped in aluminum foil and placed on a shaking board (Vibramax 100; Heidolph Instruments, Bavaria, Germany) while shaking at 300 rpm at 37 °C. At predetermined time points (0, 1, 2, 3, 4, 5 and 6 h), aliquots of 100 µL were withdrawn from each acceptor compartment and replaced with the same volume of preheated buffer. In order to hydrolyze FDA to sodium fluorescein, 10 µL of 5 M NaOH was added to each sample and incubated for 30 min. The fluorescence intensity was measured in 96-well plate at λex = 480 nm and λem = 520 nm using a microplate reader (Tecan Spark®, Tecan Trading AG, Zurich, Switzerland). The amount of permeated SEDDS was calculated in relation to a 100% reference value and under cumulative correlations of previously removed samples.

2.2.7. Enzyme-responsive change in zeta potential

The change in zeta potential of p-Ser-OA loaded SEDDS was investigated in the presence as well as in the absence of isolated AP. Accordingly, 100 µL of isolated AP (10 U/mL) was added to 10 mL of p-Ser-OA loaded SEDDS diluted 1:1000 in 100 mM HEPES buffer pH 7 containing 5 mM $MgCl_2$ and 0.2 mM $ZnCl_2$. The solution was incubated at 37 °C under constant shaking at 400 rpm for 6 h. Zeta potential was measured at predetermined time points (0, 1, 2, 3, 4, 5 and 6 h). As a control, zeta potential was measured without the addition of AP.

2.2.8. Determination of primary amino substructures

The amino substructures flipped out on the surface of the oily droplets heading into the hydrophilic phase after the cleavage of the phosphate substructures by AP. The quantity of primary amino substructures on the surface of oily droplets in the presence as well as in the absence of isolated AP was investigated by TNBS assay. Briefly, 10 mL of p-Ser-OA loaded SEDDS diluted 1:1000 in 100 mM HEPES buffer pH 7 containing 5 mM $MgCl_2$ and 0.2 mM $ZnCl_2$ were incubated with 100 µL of isolated AP (10 U/mL). At predetermined time points, aliquots of 70 µL were withdrawn. Thereafter, 70 µL of TNBS reagent (0.1% TNBS in 8% $NaHCO_3$) was added while shaking at 300 rpm for

1.5 h at 37 °C. Aliquots of 100 µL were transferred to a 96 well microtiter plate and absorbance was measured at 420 nm with a microplate reader. The quantity of primary amino groups on the surface of oily droplets was quantified using a standard curve with an increasing amount of L-cysteine hydrochloride. As a control, p-Ser-OA loaded SEDDS were incubated without isolated AP.

2.2.9. In vitro cellular uptake studies

For cellular uptake study, FDA labeled SEDDS as described above were incubated with Caco-2 cell monolayer according to an already established method [18]. In brief, Caco-2 cells in a concentration of 2.5×10^4 cells/well were seeded in a 24-well plate. After accomplishment of confluence monolayer, Caco-2 cells were washed twice with preheated HBS and incubated with HBS or phosphatase inhibitor (1% v/v) at pH 7 for 1 h. Cells were washed twice with HBS and 500 µL of FDA labeled p-Ser-OA loaded SEDDS diluted 1:1000 in HBS was added to cells and incubated for 2 and 4 h. In parallel, test samples were also applied to cells treated with phosphatase inhibitor. After incubation, cells were washed and 500 µL of HBS was added in each well except the positive control wells. Thereafter, cells were lysed by the addition of 200 µL of 2% Triton X-100 solution in 5 M NaOH for 30 min in order to hydrolyze FDA to obtain sodium fluorescein. The lysis treatment without the removal of SEDDS was used as positive control (100%) and cells incubated with buffer only represented the negative control (0%). Aliquots were transferred to 96-well plate and the fluorescence intensity of lysate corresponding to the uptake efficiency was calculated using a microplate reader at λex = 480 nm and λem = 520 nm. Cellular uptake was calculated using Eq. (2):

$$Cellular\ \ uptake\ \ efficiency = \frac{F_t - F_o}{F_{100} - F_o} \times 100 \quad (2)$$

where F_t and F_{100} represent fluorescence intensity of the lysate with and without removing test solution and F_o represents fluorescence intensity of corresponding 0%.

2.2.10. Statistical analysis

GraphPad Prism version 5.01 was used for statistical data analysis. The unpaired student's *t*-test was used for comparison between two independent groups at $^*p \leq 0.05$ for significant, $^{**}p \leq 0.01$ for very significant and $^{***}p \leq 0.001$ for highly significant. Results were expressed as means ± standard deviation (SD) of at least three experiments.

3. Results and discussion

3.1. Synthesis and characterization of phosphorylated serine-oleylamine conjugate (p-Ser-OA)

3.1.1. Synthesis of Boc-Ser-OA

The coupling of Boc-Ser to OA was achieved by amide bond formation via simple carbodiimide chemistry using EDC as illustrated in Fig. 1. FT-IR spectra of OA (Fig. 2**A**), Boc-Ser (Fig. 2**B**), Boc-Ser-OA (Fig. 2**C**) and p-Ser-OA (Fig. 2**D**) were recorded. The formation of the amide bond was evidenced by the disappearance of the signal representing the carboxylic acid at 1748 cm^{-1} in Boc-Ser (Fig. 2**B**) and appearance of the signal representing amide 1 at 1697 cm^{-1} [19] as well as the broad signal of N-H at 3322 cm^{-1} (Fig. 2**C**). The signals at 2920 cm^{-1} and 2851 cm^{-1} represented the C-H of OA (Fig. 2**A**), which also appeared in Boc-Ser-OA at 2922 cm^{-1} and 2853 cm^{-1} (Fig. 2**C**) confirming the attachment of OA with Boc-Ser via amide bond.

Additionally, the amide bond formation was verified by ^{1}H NMR analysis. The signal at 5.57 ppm was the N*H* of the Boc protected amine. The presence of the N*H* amide signal at 6.67 ppm and the change in the chemical shift of CH_2N from 2.68 ppm (OA) to 3.14 – 3.32 ppm (Boc-Ser-OA) verified the target product (Fig. 3**A**). Synthesis of Boc-Ser-OA was further confirmed by ^{13}C NMR as the signal representing the *C*H_2N group appeared at 39.5 ppm. The signal at 62.9 ppm represented the *C*-OH substructure of Boc-Ser and the ones at 129.8 ppm and 130.0 ppm the double bond of OA. Boc protective group was evidenced by the signals at 28.3, 80.6 and 156.4 ppm (**Fig. S1A)**.

3.1.2. Synthesis of p-Ser-OA

The synthesis of p-Ser-OA was carried out by the phosphorylation of the OH group of Boc-Ser-OA as depicted in Fig. 1. Within the FT-IR spectrum, signals assigned to phosphoric acid esters were shown. The signals at 945 cm^{-1} and 1009 cm^{-1} were assigned to the phosphoric acid ester (P-O), while the signal at 1064 cm^{-1} could be related to the ammonium hydrogen phosphate (1060 cm^{-1}), which might be formed upon intramolecular protonation [20]. However, it was not possible to exclude additional phosphamide formation. The broad signal of N-H was detected at 3323 cm^{-1} and the signals of C-H of OA at 2920 cm^{-1} and 2851 cm^{-1}. The presence of amide bond was confirmed by the signals at 1666 cm^{-1} (amide 1) and 1563 cm^{-1} (amide 2) (Fig. 2**D**).

In ^{1}H NMR, the signal of the methylene group at phosphates is shifted downfield compared to alcohols. The change in the chemical shift of CH_2OH (4.06–4.15 ppm) and CH_2OPO$_3$H$_2$ (3.95 ppm) (Fig. 3**A and B**) could not be used to confirm the phosphorylation, because different solvents had to be used due to the solubility of the compound. The de-protection of Boc was confirmed by disappearance of the signal representing the CH_3 of Boc (1.46 ppm in Fig. 3**A),** while it further influenced the splitting pattern of CH$_2$C*H*N (Fig. 3**B**).

The formation of p-Ser-OA was also confirmed by ^{13}C NMR analysis. The signal at 39.4 ppm (*C*H$_2$NH) verified the amide (**Fig. S1B**). Boc deprotection during phosphorylation reaction was evidenced by the disappearance of the signals at 28.3 ppm, 80.6 ppm and 156.4 ppm (**Fig. S1B**). The signal at 62.9 ppm (*C*-OH) of Boc-Ser-OA (**Fig. S1A**) shifted to 60.5 ppm due to the attachment of phosphate (*C*-OPO$_3$H$_2$) (**Fig. S1B**).

The phosphorylation was verified by ^{31}P NMR analysis. A signal at 1.07 ppm appeared, which corresponded to the phosphate ester (**Fig. S2**). The second signal at –12.45 ppm belonged to the ammonium phosphate formed between p-Ser-OA and phosphoric acid [21]. The additional formation of phosphamides could be excluded [22]. Moreover, mass spectra of p-Ser-OA were recorded. Unfortunately, it was not possible to detect the un-fragmented compound. Phosphate was split off [M^+ – 80] and only the mass of the de-protected amide could be detected which was also previously explained by Sickmann and Meyer [23].

3.2. SEDDS preparation and characterization

In order to investigate the impact of p-Ser-OA, unloaded as well as p-Ser-OA loaded SEDDS were examined regarding droplet size, PDI and zeta potential as illustrated in Table 2. Formulations (FI, FII and FIII) were loaded with 1% of p-Ser-OA. Although the lipophilic substructure of p-Ser-OA facilitated its incorporation into the oily droplets, the incorporation of higher concentrations of p-Ser-OA into SEDDS was not feasible due to insufficient solubility of the conjugate [24]. No precipitation was visually observed for the p-Ser-OA loaded SEDDS. The droplet size of FI and FIII decreased by the incorporation of conjugates compared to unloaded SEDDS due to the presence of a double bond on the lipophilic chain of the conjugate. Wang et al. described that the droplet size of nanoemulsion decreased by the introduction of a double bond in the carbon chain of the lipophilic surfactant. The presence of a double bond in the lipophilic chain of Tween 80 led to the formation of nanoemulsions with decreased droplet size compared to Span 60 having no double bond in the lipophilic carbon chain. The surfactant molecules having no double bond in the lipophilic chain would assemble more compactly at the oil/water interface compared to surfactant molecules having a double bond in the lipophilic chain. Therefore, the presence of double bond would give rise to a loosely arranged film during the process of self-emulsification favoring the development of

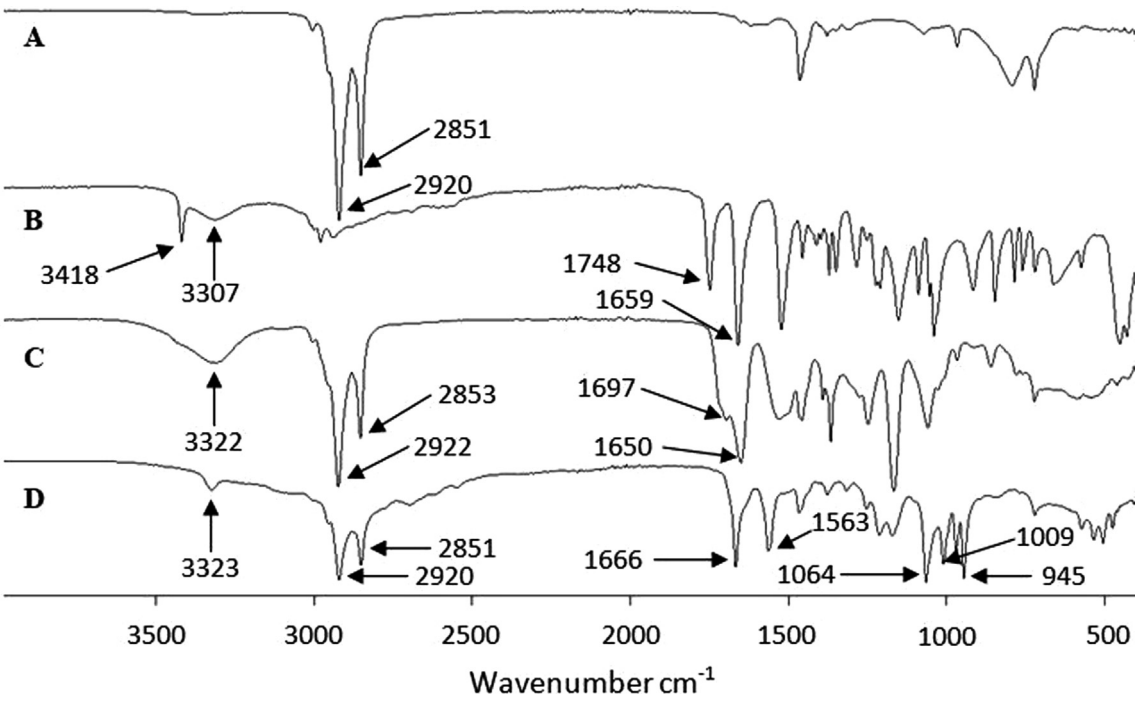

Fig. 2. FT-IR spectra of **(A)** OA, **(B)** Boc-ser, **(C)** Boc-Ser-OA and **(D)** p-Ser-OA.

nanoemulsions with small droplet size [25]. Zeta potential of FI was decreased to a higher extent after the incorporation of p-Ser-OA compared to unloaded SEDDS confirming the presence of anionic phosphate substructure on the surface of the oily droplets heading towards the aqueous phase. In contrast, the zeta potential of FII and FIII did not decrease significantly compared to FI after the incorporation of p-Ser-OA. Therefore, FI containing 1% p-Ser-AD was chosen for further analysis.

3.3. Cytotoxicity study

Drug delivery systems can cause cytotoxic effects on the epithelial membrane. The main cell type found in the small intestine is the enterocyte [26], however, Caco-2 cells have the capability to differentiate into a monolayer having the morphology and function of enterocytes [27]. Therefore, the Caco-2 cell line was chosen to investigate the cytotoxic potential of p-Ser-OA and p-Ser-OA loaded SEDDS by resazurin assay. Resazurin assay is based on cellular metabolic activity as viable cells offer the ability to metabolize resazurin (blue/non-fluorescent) to its reduced form resorufin (pink/fluorescent) [28]. It was observed that p-Ser-OA does not cause any cytotoxic effect at the concentration of 0.01% after 24 h of incubation as shown in Fig. 4. The incorporation of 1% of p-Ser-OA to SEDDS result in enhanced cytotoxic potential on Caco-2 cells. The results showed that cell viability of p-Ser-OA loaded SEDDS diluted 1:300 was 96% and reduced to 24% at SEDDS diluted 1:100 after 3 h. Lam et al. described that cytotoxicity of SEDDS on Caco-2 cells increases by the incorporation of 1% 1-decyl-3-methylimidazolium chloride loaded SEDDS diluted 0.1% compared to 0.001% 1-decyl-3-methylimidazolium chloride loaded SEDDS diluted 0.1% [29]. In contrast, p-Ser-OA loaded SEDDS diluted 1:1000 did not exhibit any cytotoxic effect within 24 h of incubation supporting the assumption that these p-Ser-OA loaded SEDDS can be considered as comparatively safe for *in vivo* applications.

3.4. Enzymatic phosphate elimination using isolated AP

AP is a ubiquitous membrane-bound endogenous glycoprotein expressed by the intestinal epithelium that catalyzes the hydrolysis of phosphate monoesters and also a transphosphorylation reaction in case of higher concentrations of phosphate acceptors. AP is a homodimeric enzyme and each catalytic site contains two zinc ions and one magnesium ion essential for its enzymatic activity. These metal ions contribute also significantly to the confirmation of the AP monomer and indirectly control subunit-subunit interactions [30,31]. Within the present study, cleavage of phosphate ester substructures on the surface of oily droplets by isolated AP was evaluated as a function of time as illustrated in Fig. 5. A fast enzymatic cleavage of the phosphate was observed within the first 60 min followed by a slow release. This behavior indicates that phosphate substructures on the surface of oily droplets were easily accessible to AP. In contrast, no significant phosphate release was observed in case of the control groups without the addition of isolated AP confirming that the cleavage of phosphate substructures from the surface of the oily droplets is entirely enzyme dependent.

3.5. Enzymatic phosphate elimination using Caco-2 cell monolayer

Caco-2 cell monolayer has been widely used to predict drug absorption in humans due to its resemblance with intestinal brush border membrane [32]. Prüfert et al. confirmed the expression of AP on Caco-2 cells by immunocytochemical analysis [33]. Yuan et al. described that Caco-2 cells on the one hand provide the predictive evidence of bioconversion of phosphate drugs and on the other hand are able to characterize drug permeability [34]. Therefore, cleavage of the phosphate substructures on the surface of p-Ser-OA loaded SEDDS was evaluated by incubating with Caco-2 cells over time. As illustrated in Fig. 6, a significant amount of phosphate (570.2 ± 40.3 nmol/g) was released from p-Ser-OA loaded SEDDS after incubation with Caco-2 cells within 6 h. The influence of enzymatic cleavage of phosphate substructures was also evaluated in the presence of phosphatase inhibitor in order to suppress AP on Caco-2 cells. As the applied phosphatase inhibitor cocktail could likely not completely suppress the enzyme activity, still a minor amount of phosphate was cleaved in the control experiment as shown in Fig. 6. These results were in good agreement with a previous study of Suchaoin et al., where a significant decrease but no entire stop in phosphate release from phosphorylated SEDDS on Caco-2 cells was observed after the addition of phosphatase

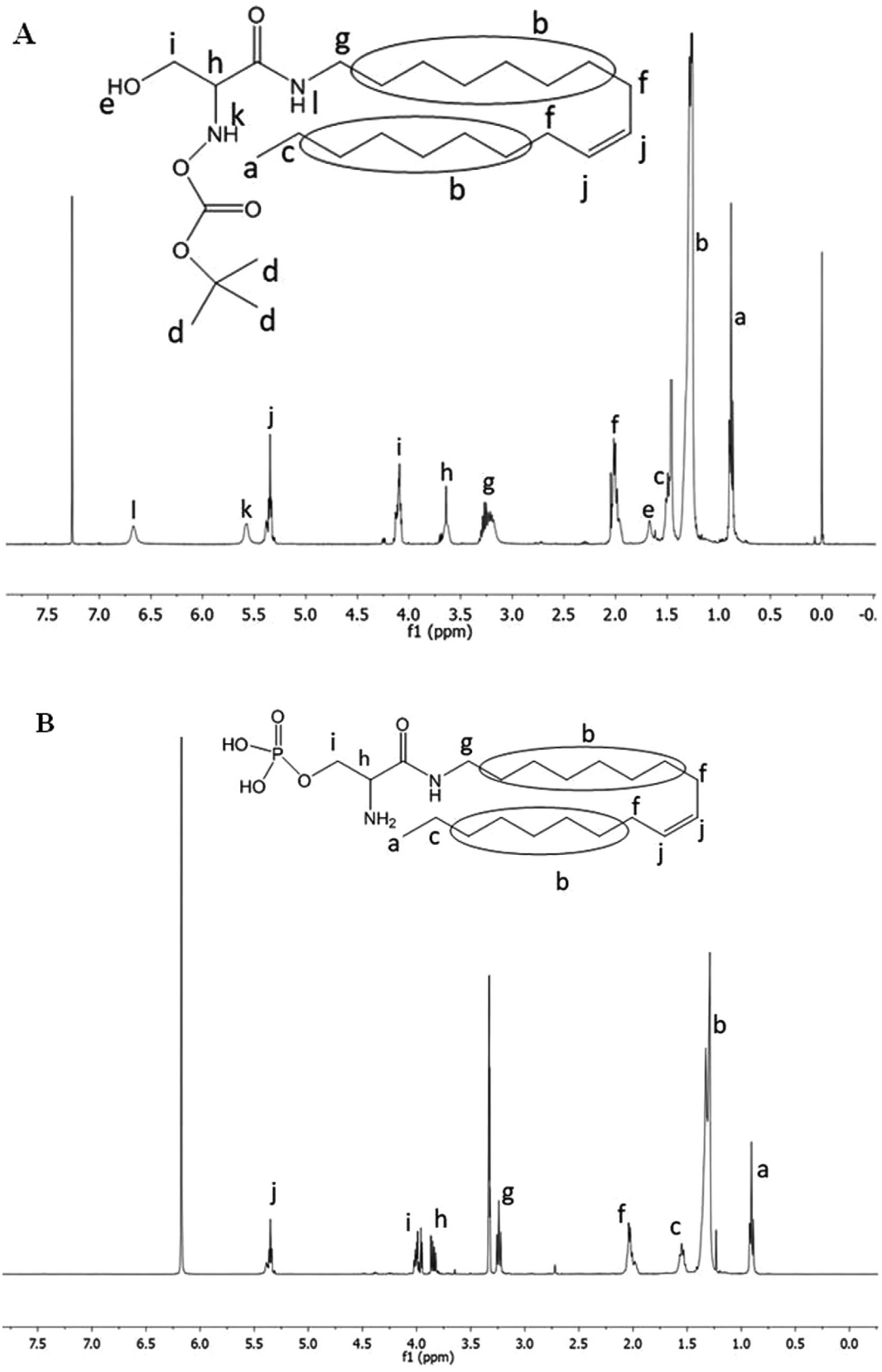

Fig. 3. ^{1}H NMR spectra of **(A)** Boc-Ser-OA in $CDCl_3$ and **(B)** p-Ser-OA in MeOD + 10% of DCl solution.

Table 2
Droplet size, PDI and zeta potential of unloaded and p-Ser-OA loaded SEDDS. Indicated values are means of at least three experiments ± SD.

Formulations	Unloaded SEDDS			p-Ser-OA loaded SEDDS 1% (v/v)		
	Droplet size (nm)	PDI	Zeta potential (mV)	Droplet size (nm)	PDI	Zeta potential (mV)
FI	53.57 ± 0.26	0.22	−2.83 ± 1.87	46.42 ± 0.35	0.29	−11.53 ± 0.24
FII	131.53 ± 1.98	0.26	−2.26 ± 2.17	139.72 ± 2.8	0.34	−6.03 ± 1.29
FIII	185.03 ± 1.16	0.30	−6.62 ± 0.70	180.02 ± 0.64	0.36	−9.14 ± 1.84

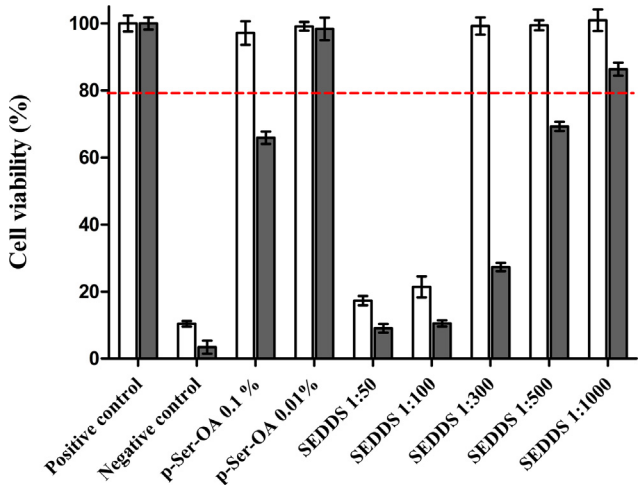

Fig. 4. Cell viability of Caco-2 cells after 3 h (white bars) and 24 h (grey bars) incubation with various concentrations of p-Ser-OA and p-Ser-OA loaded SEDDS measured by resazurin assay. Indicated values are means of at least three experiments ± SD.

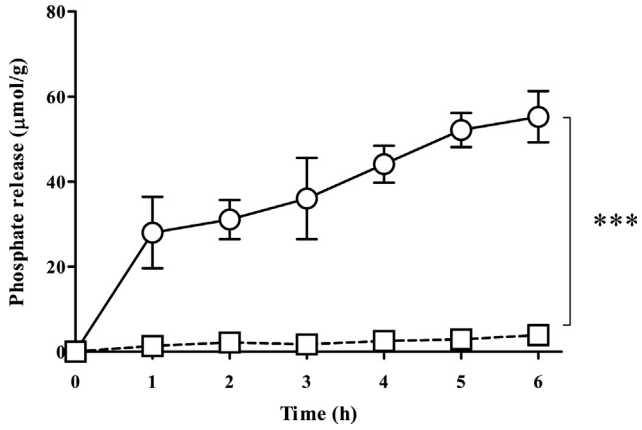

Fig. 5. Phosphate release behavior of p-Ser-OA loaded SEDDS in the presence (○) and absence (□) of 1U of isolated AP (10 U/mL) as a function of time. Indicated values are means of at least three experiments ± SD (***p ≤ 0.001).

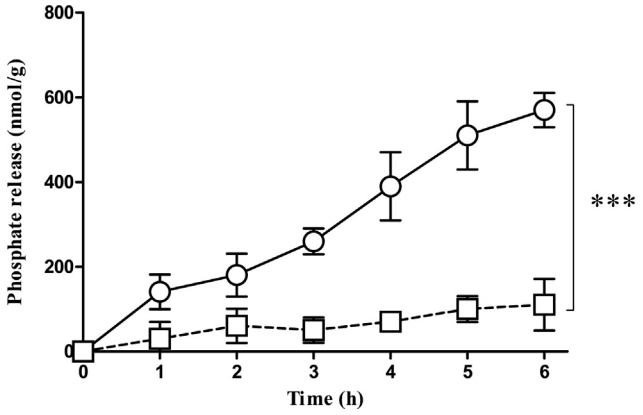

Fig. 6. Phosphate release behavior from p-Ser-OA loaded SEDDS mediated by enzymatic cleavage with AP expressed on Caco-2 cell monolayer as a function of time. Caco-2 cells were incubated with p-Ser-OA loaded SEDDS diluted 1:1000 in 25 mM HBS pH 7.4 in the presence of (□) and absence (○) of phosphatase inhibitor cocktail. Indicated values are means of at least three experiments ± SD (***p ≤ 0.001).

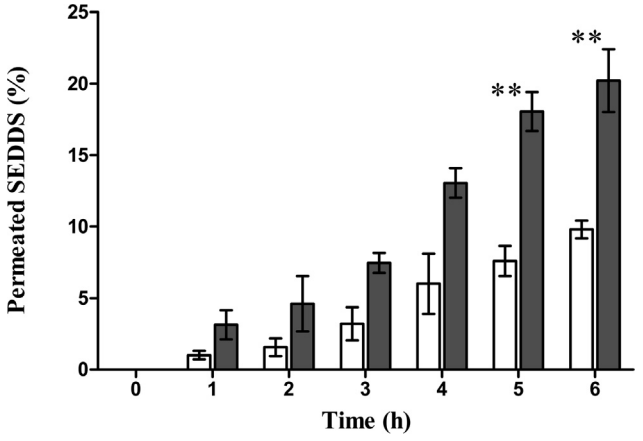

Fig. 7. Mucus permeation of FDA labeled p-Ser-OA loaded SEDDS pretreated with (white bars) and without (grey bars) 1U of isolated AP (10U/mL) through Transwell chambers at 37 °C for 6 h. Indicated values are means of at least three experiments ± SD (**p ≤ 0.01).

inhibitors [13].

3.6. Mucus permeation behavior of SEDDS

In order to permeate the mucus gel layer, nanocarriers have to possess a hydrophilic and negatively charged surface to reduce the hydrophobic entrapment and electrostatic adhesive interactions with mucus. The mucus gel layer is an adhesive and viscoelastic gel that is predominantly composed of reversibly cross-linked anionic substructures of mucin fibers secreted from goblet cells and submucosal glands [35]. The interaction between the net charge of droplets and mucin hydrogel strongly influences the transport through mucus gel layer [36]. In the present study, porcine intestinal mucus was chosen as in vitro model for mucus permeation studies due to the resemblance with human intestinal mucus in structure as well as in molecular weight [37]. The amount of permeated SEDDS was investigated over 6 h by using Transwell insert method as illustrated in Fig. 7. Transwell insert method was chosen for mucus permeation study as this method contains a single membrane system which is much closer to the *in vivo* condition [17]. p-Ser-OA loaded SEDDS exhibit 2-fold higher mucus permeation compared to p-Ser-OA loaded SEDDS pretreated with isolated AP. Suchaoin et al. described a similar mucus permeation behavior of negatively charged phosphorylated SEDDS compared to SEDDS pretreated with isolated AP [13].

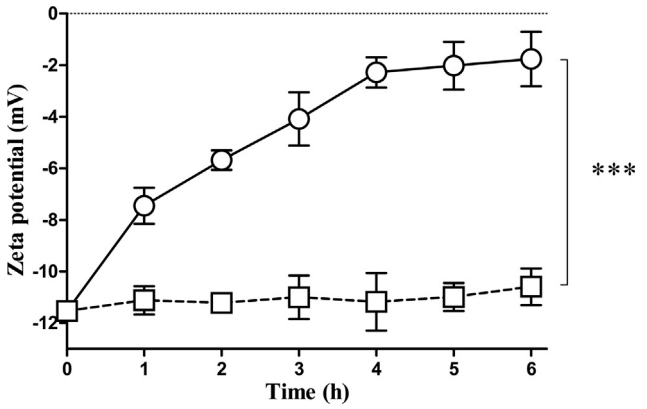

Fig. 8. Zeta potential change of p-Ser-OA loaded SEDDS in the presence (○) and absence (□) of 1U of isolated AP (10U/mL) as function of time. Indicated values are means of at least three experiments ± SD (***p ≤ 0.001).

3.7. Enzyme-induced change in zeta potential

Having proven that p-Ser-OA loaded SEDDS can permeate the mucus gel layer to a comparatively higher extend, however, their ability to overcome the epithelial barrier remained to be investigated. The phosphate substructures on the surface of the oily droplets were considered to change their zeta potential through de-phosphorylation by AP expressed in the intestinal epithelium. Therefore, the impact of phosphate cleavage on the change in zeta potential of p-Ser-OA loaded SEDDS using isolated AP was evaluated. As shown in Fig. 8, a change in zeta potential from −11.53 mV to −2.04 mV was found within 6 h of incubation with AP whereas no significant change in zeta potential was observed in case of the control groups. Griesser et al. observed a change in zeta potential of phosphorylated- hydroxypropyl starch loaded SEDDS from −6.5 mV to +1.0 mV after incubation with isolated AP [38]. Similarly, Wu et al. reported a change in zeta potential of poly (lactic-co-glycolic acid) nanoparticles containing octa-arginine and phosphoserine from −1.87 mV to +7.37 mV after incubation with isolated AP [35].

3.8. Determination of primary amino substructures

After the cleavage of the hydrophilic phosphate substructures, the polar amino substructures flipped out of the oily phase resulting in a change in zeta potential. The amino groups play a significant role in cellular uptake via endocytosis on the cell membrane by likely interacting with heparin sulfate proteoglycans being responsible for the

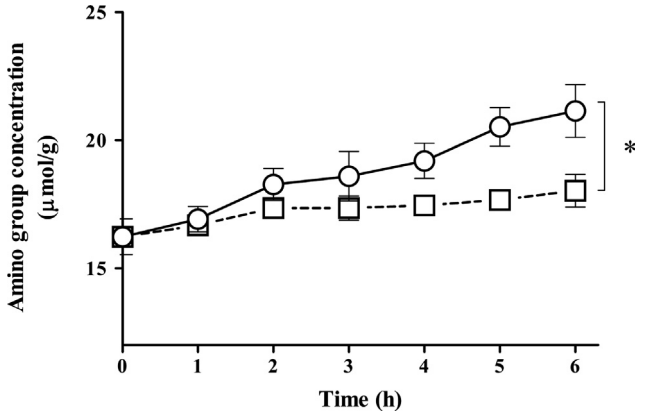

Fig. 9. Concentration of amino groups on p-Ser-OA loaded SEDDS in the presence (○) and absence (□) of 1U of isolated AP (10U/mL) as a function of time. Indicated values are the means of at least three experiments ± standard deviation (*p ≤ 0.05).

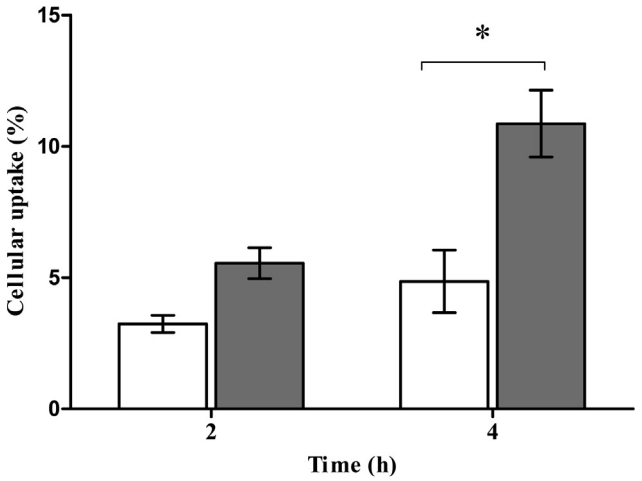

Fig. 10. Cellular uptake studies of FDA labeled p-Ser-OA loaded SEDDS in the presence (white bars) and absence (grey bars) of 1% phosphatase inhibitor cocktail. Indicated values are means of at least three experiments ± SD (*p ≤ 0.05).

uptake of cationic cell-penetrating peptides [39]. The concentration of amino substructures that flipped out to the surface of p-Ser-OA loaded SEDDS was quantified after cleavage of the hydrophilic phosphate substructure by AP as illustrated in Fig. 9. The concentration of primary amino groups on surface of the oily droplets was increased significantly over time. Salimi et al. observed a similar behavior where amino groups on the surface of phosphotyrosine octadecylamine loaded SEDDS flipped out at a concentration of 7.19 ± 0.20 to 11.02 ± 0.35 µmol/g after incubation with isolated AP [14]. Sharifi et al. also reported that the primary amino group of a Janus-headed surfactant migrate on the surface of oily droplets after cleavage of phosphate substructures by AP over time [40].

3.9. In vitro cellular uptake studies

Absorption barrier of epithelium is another challenging obstacle to mucosal delivery of nanocarriers, especially those having negatively charged and hydrophilic substructures on the surface [41]. The internalization or uptake of p-Ser-OA loaded SEDDS was evaluated on Caco-2 cells in the presence or absence of phosphatase inhibitor. The uptake was almost 2-fold increased in the absence of phosphatase inhibitors as illustrated in Fig. 10. In the presence of phosphatase inhibitor, the surface of oily droplets covered by phosphate substructures shielding interactions of amino substructures with heparin sulfate of the cell membrane resulted in decreased cellular uptake. Wu et al. observed a 71.4% substantially reduced relative uptake of poly(lactic-co-glycolic acid) nanoparticles containing octa-arginine and phosphoserine in the presence of phosphatase inhibitor [35]. Le-Vinh et al. described that positively charged chitosan-stearic acid micelles exhibit 3.2-fold higher cellular uptake than phosphorylated chitosan-stearic acid micelles [12].

4. Conclusion

Within this study, zeta potential changing SEDDS was successfully developed via a flip-flop mechanism in order to improve their mucus permeating and cellular uptake properties. SEDDS exhibiting a highly negative zeta potential due to hydrophilic phosphate substructures on the surface result in enhanced mucus permeation. At epithelial membrane, cleavage of these phosphate substructures of SEDDS by AP causes the amino substructures to flip out on the surface of the oily droplets mediating a change in zeta potential that enhances cellular uptake. Results of this study suggest that SEDDS changing their zeta potential via a flip-flop mechanism are a promising tool to sequentially

overcome the mucus and epithelial barrier.

Declaration of Competing Interest

There are no conflicts of interest to declare.

Acknowledgement

The authors are thankful and would like to extend acknowledgment to the Higher Education Commission (HEC), Pakistan and the Austrian Agency for International Cooperation in Education and Research (ÖAD), Austria for their support. The Austrian Research Promotion Agency FFG (West Austrian BioNMR 858017) is kindly acknowledged. The research leading to these results has received funding from the Austrian Science Fund (FWF), Austria under the project number P30268-B30.

Appendix A. Supplementary material

Supplementary data to this article can be found online at https://doi.org/10.1016/j.ejpb.2019.09.007.

References

[1] C. Menzel, A. Bernkop-Schnuerch, Enzyme decorated drug carriers: targeted swords to cleave and overcome the mucus barrier, Adv. Drug Deliv. Rev. 124 (2018) 164–174.
[2] H. Zhang, J. Zhang, J.B. Streisand, Oral mucosal drug delivery, Clin. Pharmacokinet. 41 (9) (2002) 661–680.
[3] J.D. Du, et al., A novel approach to enhance the mucoadhesion of lipid drug nanocarriers for improved drug delivery to the buccal mucosa, Int. J. Pharm. 471 (1–2) (2014) 358–365.
[4] M. Liu, et al., Core–shell stability of nanoparticles plays an important role for overcoming the intestinal mucus and epithelium barrier, J. Mater. Chem. B 4 (35) (2016) 5831–5841.
[5] M.H. Asim, et al., S-protected thiolated cyclodextrins as mucoadhesive oligomers for drug delivery, J. Colloid Interface Sci. 531 (2018) 261–268.
[6] S. Oh, S. Borrós, Mucoadhesion vs mucus permeability of thiolated chitosan polymers and their resulting nanoparticles using a quartz crystal microbalance with dissipation (QCM-D), Colloids Surf., B 147 (2016) 434–441.
[7] S. Maher, R.J. Mrsny, D.J. Brayden, Intestinal permeation enhancers for oral peptide delivery, Adv. Drug Deliv. Rev. 106 (2016) 277–319.
[8] M. Abdulkarim, P.K. Sharma, M. Gumbleton, Self-emulsifying drug delivery system: mucus permeation and innovative quantification technologies, Adv. Drug Deliv. Rev. (2019).
[9] W. Shan, et al., Enhanced oral delivery of protein drugs using zwitterion-functionalized nanoparticles to overcome both the diffusion and absorption barriers, ACS Appl. Mater. Interfaces 8 (38) (2016) 25444–25453.
[10] I. Nazir, et al., Surface phosphorylation of nanoparticles by hexokinase: a powerful tool for cellular uptake improvement, J. Colloid Interface Sci. 516 (2018) 384–391.
[11] G. Perera, et al., Development of phosphorylated nanoparticles as zeta potential inverting systems, Eur. J. Pharm. Biopharm. 97 (2015) 250–256.
[12] B. Le-Vinh, et al., Chitosan based micelle with zeta potential changing property for effective mucosal drug delivery, Int. J. Biol. Macromol. 133 (2019) 647–655.
[13] W. Suchaoin, et al., Development and in vitro evaluation of zeta potential changing self-emulsifying drug delivery systems for enhanced mucus permeation, Int. J. Pharm. 510 (1) (2016) 255–262.
[14] E. Salimi, et al., Self-emulsifying drug delivery systems changing their zeta potential via a flip-flop mechanism, Int. J. Pharm. 550 (1–2) (2018) 200–206.
[15] I. Nazir, et al., Self-emulsifying drug delivery systems: impact of stability of hydrophobic ion pairs on drug release, Int. J. Pharm. 561 (2019) 197–205.
[16] I. Shahzadi, et al., Trypsin decorated self-emulsifying drug delivery systems (SEDDS): key to enhanced mucus permeation, J. Colloid Interface Sci. 531 (2018) 253–260.
[17] H. Friedl, et al., Development and evaluation of a novel mucus diffusion test system approved by self-nanoemulsifying drug delivery systems, J. Pharm. Sci. 102 (12) (2013) 4406–4413.
[18] A. Mahmood, et al., Cell-penetrating self-nanoemulsifying drug delivery systems (SNEDDS) for oral gene delivery, Exp. Opin. Drug Deliv. 13 (11) (2016) 1503–1512.
[19] S. Cai, B.R. Singh, Identification of β-turn and random coil amide III infrared bands for secondary structure estimation of proteins, Biophys. Chem. 80 (1) (1999) 7–20.
[20] F.A. Miller, C.H. Wilkins, Infrared spectra and characteristic frequencies of inorganic ions, Anal. Chem. 24 (8) (1952) 1253–1294.
[21] Z. Wittmann, Z. Kovacs, Phosphorus-31 nuclear magnetic resonance chemical shifts of phosphoric acid derivatives, Talanta 32 (7) (1985) 581–582.
[22] L.D. Quin, A.J. Williams, Practical interpretation of P-31 NMR spectra and computer assisted structure verification, Advanced Chemistry Development Toronto, 2004.
[23] A. Sickmann, H.E. Meyer, Phosphoamino acid analysis, PROTEOMICS: Int. Ed. 1 (2) (2001) 200–206.
[24] N. Thomas, et al., In vitro and in vivo performance of novel supersaturated self-nanoemulsifying drug delivery systems (super-SNEDDS), J. Contr. Rel. 160 (1) (2012) 25–32.
[25] L. Wang, et al., Design and optimization of a new self-nanoemulsifying drug delivery system, J. Colloid Interface Sci. 330 (2) (2009) 443–448.
[26] P. Simon-Assmann, et al., In vitro models of intestinal epithelial cell differentiation, Cell Biol. Toxicol. 23 (4) (2007) 241–256.
[27] A.L. Kauffman, et al., Alternative functional in vitro models of human intestinal epithelia, Front. Pharmacol. 4 (2013) 79.
[28] H.-X. Zhang, G.-H. Du, J.-T. Zhang, Assay of mitochondrial functions by resazurin in vitro, Acta Pharmacol. Sin. 25 (3) (2004) 385–389.
[29] H.T. Lam, et al., Self-emulsifying drug delivery systems and cationic surfactants: do they potentiate each other in cytotoxicity? J. Pharm. Pharmacol. 71 (2) (2019) 156–166.
[30] J. Millan, Alkaline phosphatases structure, substrate specificity and functional relatedness to other members of a large superfamily of enzymes Purinergic, Signal 2 (2006) 335–341.
[31] M.F. Hoylaerts, T. Manes, J.L. Millán, Mammalian alkaline phosphatases are allosteric enzymes, J. Biol. Chem. 272 (36) (1997) 22781–22787.
[32] T. Heimbach, et al., Absorption rate limit considerations for oral phosphate prodrugs, Pharm. Res. 20 (6) (2003) 848–856.
[33] F. Prüfert, et al., ζ potential changing nanoparticles as cystic fibrosis transmembrane conductance regulator gene delivery system: an in vitro evaluation, Nanomedicine 12 (22) (2017) 2713–2724.
[34] H. Yuan, N. Li, Y. Lai, Evaluation of in vitro models for screening alkaline phosphatase-mediated bioconversion of phosphate ester prodrugs, Drug Metab. Dispos. 37 (7) (2009) 1443–1447.
[35] J. Wu, et al., Biomimetic viruslike and charge reversible nanoparticles to sequentially overcome mucus and epithelial barriers for oral insulin delivery, ACS Appl. Mater. Interfaces 10 (12) (2018) 9916–9928.
[36] I.P. de Sousa, et al., Mucus permeating carriers: formulation and characterization of highly densely charged nanoparticles, Eur. J. Pharm. Biopharm. 97 (2015) 273–279.
[37] A.-C. Groo, F. Lagarce, Mucus models to evaluate nanomedicines for diffusion, Drug Discov. Today 19 (8) (2014) 1097–1108.
[38] J. Griesser, et al., Zeta potential changing self-emulsifying drug delivery systems containing phosphorylated polysaccharides, Eur. J. Pharm. Biopharm. 119 (2017) 264–270.
[39] S.K. Lai, Y.-Y. Wang, J. Hanes, Mucus-penetrating nanoparticles for drug and gene delivery to mucosal tissues, Adv. Drug Deliv. Rev. 61 (2) (2009) 158–171.
[40] F. Sharifi, et al., Zeta potential changing self-emulsifying drug delivery systems utilizing a novel Janus-headed surfactant: a promising strategy for enhanced mucus permeation, J. Mol. Liq. (2019) 111285.
[41] A. Lechanteur, J. Das Neves, B. Sarmento, The role of mucus in cell-based models used to screen mucosal drug delivery, Adv. Drug Deliv. Rev. 124 (2018) 50–63.